Performance Evaluation of 2D Adaptive Prediction Filters for Detection of Small Objects in Image Data[*]

Tarun Soni, James R. Zeidler[†], and Walter H. Ku

Department of Electrical and Computer Engineering

University of California at San Diego, La Jolla, CA 92093-0407

[†]Also with: Naval Command, Control and Ocean Surveillance Center,

R.D.T. & E. Division, Code 804, San Diego, CA 92152-5000

EDICS 1.3

Abstract

This paper studies the performance of two dimensional least mean square(TDLMS) adaptive filters as prewhitening filters for the detection of small objects in image data. The object of interest is assumed to have a very small spatial spread and is obscured by correlated clutter of much larger spatial extent. The correlated clutter is predicted and subtracted from the input signal, leaving components of the spatially small signal in the residual output. The receiver operating characteristics of a detection system augmented by a TDLMS prewhitening filter are plotted using Monte-Carlo techniques. It is shown that such a detector has better operating characteristics than a conventional matched filter in the presence of correlated clutter. For very low signal to background ratios, TDLMS based detection systems show a considerable reduction in the number of false alarms. The output energy in both the residual and prediction channels of such filters is shown to be dependent on the correlation length of the various components in the input signal. False alarm reduction and detection gains obtained by using this detection scheme on thermal infrared sensor data with known object positions is presented.

1

1 Introduction

This paper addresses the problem of detecting dim objects with very small spatial extent that are masked by spatially large clutter in image data. Applications where this is of interest include the detection of tumors and other irregularities in medical images and target detection in infrared sensor data. Prediction based methods which rely on the accuracy of specified image representation models are often applied to such applications [1–3].

A number of models have been proposed for clutter representation [4]. Takken et. al. [5–7] developed a spatial filter based on least mean square optimization to maximize the signal to clutter ratio for a known and fixed clutter environment. A local demeaning filter has been used to track the non-stationary mean in an image by Reed et. al. in [8,9]. Chen et. al. [8] modeled the underlying clutter and noise after local demeaning as a whitened Gaussian random process and developed a constant false alarm rate detector using the generalized maximum likelihood ratio. Wang [10] and Adridges et. al. [11] use adaptive techniques to obtain a local estimate of spatially varying clutter. Other infrared systems [8, 12, 13] use multispectral data and multi-dimensional matched filtering techniques based on an underlying model of the data.

One dimensional adaptive linear prediction filters have been applied to the detection of narrow band signals embedded in non-stationary noise as well as to the removal of narrow band interference from broad band data [14–18]. In the first case a narrow band signal of interest is extracted from the prediction channel of the adaptive filter. In the second case the broad band signal of interest is extracted from the residual error of the adaptive filter [14,16]. Adaptive filters analogous to the LMS and lattice implementations in one dimension, have been recently extended to two dimensions with applications in image processing [19–23]. These algorithms update the filter weights based on the spatial coherence between the signal and noise components of the data and minimize the variance of the prediction error (residual) without explicit assumptions about the noise statistics.

In this paper the performance of two dimensional least mean square (TDLMS) adaptive filters as whitening filters for the detection of signals of small spatial extent embedded in spatially distributed clutter is examined. In section 2 the TDLMS adaptive filter used in a line enhancer configuration is described. In section 3, the performance of a detection

system augmented by a TDLMS prewhitening filter is studied for narrowband clutter in images. The optimal weights for sinusoidal inputs are derived and the receiver operating characteristics are plotted using Monte-Carlo techniques. In section 4 the filter is applied towards the detection of point objects embedded in clouds. The reduction in false alarms due to prewhitening is described. Section 5 describes the application of the TDLMS based filter on thermal infrared multispectral (TIMS) data which contains small objects at known locations.

2 The Two Dimensional Adaptive Whitening Filter

The optimal detector for known signals in stationary correlated noise is a two stage detector with the first stage being a whitening filter [24]. For unknown and possibly nonstationary noise and clutter, an adaptive filter can be used as the first stage whitening filter(Fig.1) as discussed in [14–16] .

The Least Mean Square(LMS) algorithm can be applied as a predictor for whitening the correlated clutter in an image as shown in Fig.2. The distinction between clutter and noise in this application is based on the predictability of the two. The components of the background that are stochastic random processes will be called noise and the deterministic component of the background which are not part of the signal will be called clutter.

The TDLMS adaptive filter described in [19] predicts an image pixel as a weighted average of a small window of pixels as

$$\mathbf{Y}(m,n) = \sum_{l=0}^{N-1} \sum_{k=0}^{N-1} \mathbf{W}_j(l,k)\mathbf{X}(m-l,n-k) \qquad\qquad m,n = 0,\ldots,M-1 \qquad (1)$$

where, $\mathbf{X}$ is the input image of size $M \times M$, Y is the predicted image and $\mathbf{W}_j$ is the weight matrix at the jth iteration. The window size (and hence the weight matrix) is $N \times N$. If the image is scanned lexicographically, $j = mM + n$. The predicted pixel value is compared with a reference image ,$\mathbf{D}(m,n)$, which is a shifted version of the primary image in the line enhancer configuration. The error is found as

$$\mathbf{E}(m,n) = \epsilon_j = \mathbf{D}(m,n) - \mathbf{Y}(m,n). \qquad (2)$$

The adaptation algorithm minimizes the expected value of this mean square error over the complete image. An ideal Wiener filter implementation requires knowledge of the autocorrelation and the cross-correlation between the various regions of interest in the image and assumes stationary characteristics. Under such conditions, the ideal filter weights are then given by the two dimensional Wiener-Hopf equation as

$$\mathbf{P}(l,k) = \sum_{p=0}^{N-1} \sum_{q=0}^{N-1} \mathbf{W}^*(p,q)\mathbf{R}(l-p,k-q) \qquad l,k = 0,\ldots,N-1 \qquad (3)$$

where $\mathbf{W}^*$ are the optimum filter weights, $\mathbf{P}$ is the crosscorrelation matrix defined by

$$\mathbf{P} = \begin{bmatrix} \mathcal{E}\left(\mathbf{D}(m,n)\mathbf{X}(m,n)\right) & \cdots & \mathcal{E}\left(\mathbf{D}(m,n)\mathbf{X}(m,n-N+1)\right) \\ \vdots & \vdots & \vdots \\ \mathcal{E}\left(\mathbf{D}(m,n)\mathbf{X}(m-N+1,n)\right) & \cdots & \mathcal{E}\left(\mathbf{D}(m,n)\mathbf{X}(m-N+1,n-N+1)\right) \end{bmatrix}$$

and $\mathbf{R}$ is the input autocorrelation matrix with elements defined by

$$\mathbf{R}(l-p,k-q) = \mathcal{E}\left(\mathbf{X}(m-l,n-k)\mathbf{X}(m-p,n-q)\right). \qquad (4)$$

In the absence of any knowledge of these statistics of the input, the LMS algorithm uses instantaneous estimates. Then, the steepest descent algorithm leads to the weight update equation

$$\mathbf{W}_{j+1}(l,k) = \mathbf{W}_j + \mu\epsilon_j\mathbf{X}(m-l,n-k) \qquad l,k = 0,\ldots,N-1 \qquad (5)$$

Separation of the clutter and signal of interest is accomplished by predicting one of them and subtracting it from the input channel. Since the image is clutter dominated, with the correlated clutter having more energy than the signal of interest, the adaptive filter is made to adapt to the clutter, and predict it. The residual or error channel then contains the signal of interest in white noise. In our implementation a causal window with quarter plane support and a left to right lexicographic scan were used, though other schemes for prediction and update can be used. For example, Ohki et. al. [20] suggest a technique for updating the filter coefficients in both directions.

The TDLMS adaptive filter has a very low computational complexity. For a $w \times w$ sized TDLMS filter window, the computations required per pixel of the input image are $O(w^2)$ additions and $O(w^2)$ multiplications This makes it a viable choice for real time systems implementations.

3 Detection Performance for Point Objects in Narrow Band Clutter and Noise

In this section we describe the performance of the two stage detection system described in section 2 for the detection of point objects in narrow band noise and clutter.

The optimal filter weights of the TDLMS adaptive filter are given by the two dimensional Wiener-Hopf equation [19] as

$$\sum_{p=0}^{L-1} \sum_{q=0}^{L-1} \mathbf{W}^*(p,q)\mathbf{R}(p-l,q-k) = \mathbf{P}(l,k) \qquad \forall\, l,k \in [0, L-1] \qquad (6)$$

where the filter window is assumed to be $L \times L$ and the auto correlation and cross correlation matrices are given by

$$\mathbf{R}(p-l,q-k) = \mathcal{E}\left(\mathbf{X}(m-l,n-k)\mathbf{X}(m-p,n-q)\right) \qquad (7)$$

and

$$\mathbf{P}(l,k) = \mathcal{E}\left(\mathbf{D}(m,n)\mathbf{X}(m-l,n-k)\right). \qquad (8)$$

Here $\mathbf{X}$ is the primary input and $\mathbf{D}$ is the reference input. For the prediction filter configuration shown in Fig.2, the reference is a delayed version of the primary and hence the 2-D Wiener Hopf equation can be written as

$$\sum_{p=0}^{L-1} \sum_{q=0}^{L-1} \mathbf{W}^*(p,q)\mathbf{R}(p-l,q-k) = \mathbf{R}(l+\Delta_x, k+\Delta_y) \qquad \forall\, l,k \in [0, L-1] \qquad (9)$$

where (Δ_x, Δ_y) are the delays in the two directions. All the simulations in this paper were run with $\Delta_x = \Delta_y = 1$ which corresponds to "one step prediction".

An ideal narrow band clutter in the form of a two dimensional sinusoid with random

phase is assumed. For such a two-dimensional sinusoid in zero mean white Gaussian noise, the autocorrelation matrix can be written as

$$\mathcal{E}\left(\mathbf{X}(m-p_1, n-q_1)\mathbf{X}(m-p_2, n-q_2)\right) =$$

$$\sigma_0^2 \delta(p_1 - p_2, q_1 - q_2) + \sigma_s^2 cos\left(\omega_x(p_1 - p_2) + \omega_y(q_1 - q_2)\right) \tag{10}$$

where σ_0 is the power of the white noise and σ_s is the power of the sinusoid.

To solve for the optimal weights given by Eq.9, we use the method of undetermined coefficients used in [25]. For a 2-D sinusoidal input, the weights are assumed to be of the form

$$\mathbf{W}^*(p, q) = \alpha_x^T \mathbf{A} \alpha_y \tag{11}$$

where

$$\begin{aligned}
\alpha_x^T &= \left[e^{j\omega_x p} \; e^{-j\omega_x p} \right] \\
\alpha_y^T &= \left[e^{j\omega_y q} \; e^{-j\omega_y q} \right]
\end{aligned} \tag{12}$$

and $\mathbf{A}$ is the matrix of coefficients as

$$\mathbf{A} = \begin{pmatrix} A_{11} & A_{12} \\ A_{21} & A_{22} \end{pmatrix}. \tag{13}$$

When equations 10 and 11 are applied to the 2-D Wiener-Hopf equations given by Eq.9, we get

$$
\begin{aligned}
e^{-j\omega_x l}e^{-j\omega_y k} \quad & \left(A_{22}\sigma_0^2 + A_{22}L^2\frac{\sigma_s^2}{2} + A_{12}L\gamma_x\frac{\sigma_s^2}{2} + A_{21}L\gamma_y\frac{\sigma_s^2}{2} + A_{11}\gamma_x\gamma_y\frac{\sigma_s^2}{2} \right) \\
+ e^{j\omega_x l}e^{j\omega_y k} \quad & \left(A_{11}\sigma_0^2 + A_{11}L^2\frac{\sigma_s^2}{2} + A_{12}Le^{-2j\omega_y(L-1)}\gamma_y\frac{\sigma_s^2}{2} + \right. \\
& \left. A_{21}Le^{-2j\omega_x(L-1)}\gamma_x\frac{\sigma_s^2}{2} + A_{22}e^{-2j\omega_x(L-1)}e^{-2j\omega_y(L-1)}\gamma_x\gamma_y\frac{\sigma_s^2}{2} \right) \\
+ e^{j\omega_x l}e^{-j\omega_y k} \quad & \left(A_{12}\sigma_0^2 \right) \\
+ e^{-j\omega_x l}e^{j\omega_y k} \quad & \left(A_{21}\sigma_0^2 \right) \\
= & \\
e^{j\omega_x l}e^{j\omega_y k} \quad & \left(\frac{\sigma_s^2}{2}e^{j\omega_x \Delta_x}e^{j\omega_y \Delta_y} \right) \\
e^{-j\omega_x l}e^{-j\omega_y k} \quad & \left(\frac{\sigma_s^2}{2}e^{-j\omega_x \Delta_x}e^{-j\omega_y \Delta_y} \right)
\end{aligned}
$$

where γ_x and γ_y are defined by

$$\gamma_x = \frac{1 - e^{2j\omega_x L}}{1 - e^{2j\omega_x}} \tag{14}$$

and

$$\gamma_y = \frac{1 - e^{2j\omega_y L}}{1 - e^{2j\omega_y}}. \tag{15}$$

On comparing the coefficients of the relevant terms we get

$$
\begin{aligned}
A_{12} &= 0 \\
A_{21} &= 0 \\
\Gamma_{11} A_{11} + A_{22} &= \frac{1}{L^2 + 2\sigma_0^2/\sigma_s^2} e^{-j\omega_x \Delta_x} e^{-j\omega_y \Delta_y} \\
A_{11} + \Gamma_{22} A_{22} &= \frac{1}{L^2 + 2\sigma_0^2/\sigma_s^2} e^{j\omega_x \Delta_x} e^{j\omega_y \Delta_y}
\end{aligned}
$$

where

$$\Gamma_{11} = \frac{1}{L^2 + 2\sigma_0^2/\sigma_s^2} \left(\frac{1 - e^{2j\omega_x L}}{1 - e^{2j\omega_x}} \right) \left(\frac{1 - e^{2j\omega_y L}}{1 - e^{2j\omega_y}} \right) \tag{16}$$

and

$$\Gamma_{22} = \frac{1}{L^2 + 2\sigma_0^2/\sigma_s^2} \left(\frac{1 - e^{-2j\omega_x L}}{1 - e^{-2j\omega_x}} \right) \left(\frac{1 - e^{-2j\omega_y L}}{1 - e^{-2j\omega_y}} \right). \tag{17}$$

Now, for all $\Gamma_{11}\Gamma_{22} \neq 1$ we can solve the set of equations given by Eq.16 to get

$$
\begin{bmatrix} A_{11} \\ A_{22} \end{bmatrix} = \frac{1}{(\Gamma_{11}\Gamma_{22} - 1)\left(L^2 + 2\sigma_0^2/\sigma_s^2\right)} \begin{bmatrix} \Gamma_{22} & -1 \\ -1 & \Gamma_{11} \end{bmatrix} \begin{bmatrix} e^{-j\omega_x \Delta_x} e^{-j\omega_y \Delta_y} \\ e^{j\omega_x \Delta_x} e^{j\omega_y \Delta_y} \end{bmatrix}. \tag{18}
$$

Thus the weights can now be written as

$$\mathbf{W}^*(p, q) = A_{11} e^{j(\omega_x p + \omega_y q)} + A_{22} e^{-j(\omega_x p + \omega_y q)}. \tag{19}$$

Further, since $\Gamma_{11} = \Gamma_{22}^*$ we have $A_{11} = A_{22}^*$, leading to

$$\mathbf{W}^*(p, q) = \rho \cos\left(\omega_x p + \omega_y q + \theta\right) \tag{20}$$

where $\rho = 2 \mid A_{11} \mid$ and $\theta = \angle A_{11}$.

To confirm this analytical expression for the optimum weights a TDLMS filter with a

7

32x32 weight matrix with a μ of 10^{-8} was applied to a two dimensional sinusoid and the weights were observed after convergence. The sinusoid was taken to have a frequency of 0.28 radians per pixel in both the axes with additive white Gaussian noise at a signal to white noise ratio of 29.59 dB. Two columns of the weight matrix are plotted in Fig.3, and the weights of the TDLMS adaptive filter agree very well with the optimum weights defined by Eq.20.

It is seen that the optimum weights are sinusoidal when the input is a stationary sinusoid. This result is similar to that obtained for a one dimensional LMS prediction filter with an input consisting of a sinusoid in white Gaussian noise [26, 27]. As in the one dimensional case, with a proper choice of μ, the TDLMS adaptive filter weights converge so as to predict the correlated component in the background.

In [28] it is shown that the weights of a one dimensional adaptive filter can be modeled as having two components: the optimal weights($\mathbf{W}^*$) and the misadjustment component($\tilde{\mathbf{W}}$). The weights of the TDLMS can be similarly modeled with $\mathbf{W}^*$ defined by Eq.20 and an additive misadjustment term. The prediction channel of the filter will then consist of four components: (1) The optimally predicted clutter, (2) The noise and spatially small signal of interest filtered by $\mathbf{W}^*$, (3) the misadjustment output due to the clutter and (4) the noise and signal of interest filtered through the misadjustment filter ($\tilde{\mathbf{W}}$). The error channel will contain components from the signal of interest and the input noise, and will also contain the misadjustment components of the clutter.

3.1 TDLMS Augmented Detection in Narrowband Noise

The receiver operating characteristics of a detector augmented by a TDLMS adaptive filter were found by Monte-Carlo simulations. The infrared signal model developed by Chan et. al. [4] was used for these simulations. This model leads to a Gaussian intensity function for the object, of the form

$$I(x, y) = \Gamma e^{-\left(\frac{(x-x_0)^2}{\sigma_x^2} + \frac{(y-y_0)^2}{\sigma_y^2}\right)} \tag{21}$$

where Γ is the maximum value of the object intensity function, (x_0, y_0) is the position of the center of the object, and (σ_x, σ_y) define the spatial spread of the object. The background,

8

C(x,y), consists of clutter and noise components of the form,

$$C(x,y) = aSin(\omega_x x + \omega_y y) + W(x,y) \tag{22}$$

where the power of the clutter component is given by $a^2/2$ and $W(x,y)$ is zero mean white Gaussian noise process of variance σ^2.

The input image then becomes

$$Y(x,y) = I(x,y) + C(x,y) \tag{23}$$

and is shown [1] in Fig.4a.

Fig.5 shows the spectrum of the input image in the two dimensional spatial frequency domain. The sinusoidal clutter contributes to the spatial spectrum of the input with a narrowband spike at the position (ω_x, ω_y) of the spatial frequency space. The signal of interest is a broadband signal with its energy spread across a wide band of spatial frequencies. Fig.6 shows the two dimensional frequency domain log magnitude plot of the output image at the residual channel of the TDLMS adaptive filter. A 3×3 window with $\mu = 1e - 6$ was used. The broadband energy of the object is seen to be present while there is a notch at the frequency of the interfering clutter, with very little energy in those frequencies. It is thus seen that the narrowband clutter has been predicted and cancelled from the input. This is also evident in Fig.4b which shows the pixel intensities of the error channel output of the TDLMS filter.

The average noise energy per pixel, N_E, in Fig.4a is given by

$$N_E = \frac{a^2}{2} + \sigma^2. \tag{24}$$

---

[1] All images in this paper are 256×256 pixels in size. They are shown with the upper left corner corresponding to the $(1,1)$ pixel and the lower right corner corresponding to the $(256, 256)$ pixel. The horizontal direction corresponds to the x axis (the first index of the image) and the vertical direction corresponds to the y axis. The intensity values for all images has been normalized to have a maximum of 255 and a minimum of 0.

The average correlation per pixel, K, in the noise can then be defined as the ratio

$$K = \frac{a^2/2}{a^2/2 + \sigma^2}.$$ (25)

And the total signal energy, S_E in the image is

$$S_E = \sum_{i=1}^{N} \sum_{j=1}^{N} \mathbf{I}^2(i,j)$$ (26)

where the image size is $N \times N$. The signal to background ratio per pixel(PSBR) in the image then becomes

$$PSBR = \frac{S_E}{N^2 * N_E}.$$ (27)

The Adaptive Clutter whitener(ACW) augmented detector was compared with a conventional matched filter for different amounts of background correlation. The filter window used was 3×3 and a $\mu = 10^{-6}$ was chosen. The amount of correlation in the background was allowed to vary while the total N_E was kept constant. Thus the PSBR was kept fixed, and the correlated component (K) in the background was increased from 0 to 1. The probability of detection and the probability of false alarm were found for both the ACW-augmented detector and the conventional matched filter and the receiver operating characteristics plotted.

The probability of detection (P_d) was found by using the detector output at the pixels where the object is known to be present and comparing it to a threshold to make a decision. 500 independent runs were used to calculate the probability of detection. The probability of false alarm (P_{fa}) was calculated by comparing the pixel output values of the same matched filter at pixel locations where the object was known to be absent. The threshold was selected across the range of the matched filter outputs to get different false alarm and detection rates. In these simulations the P_{fa} was found using the matched filter output at 25 random pixels in the image (sufficiently far away from the object location) for 500 runs giving a total of 12500 samples. A very low PSBR and consequently a very high P_{fa} was used to reduce the number of computations required to calculate the P_{fa}.

3.2 Operating Characteristics of the TDLMS Augmented Detector

Fig.7 shows the receiver operating characteristics(ROCs) of the two detectors. When the background consists of white noise (ie, $K = 0$), the conventional matched filter has better operating characteristics than the augmented matched filter. This is expected, since the misadjustment in the TDLMS augmenting filter will add to the white noise in the background. Further, as K increases, the performance of both the detectors is seen to degrade and the operating characteristics move towards the right of the plot, signifying a higher P_{fa} for a given P_d. However, the performance of the conventional matched filter degrades much more than that of the ACW augmented filter. The operating characteristics of the conventional matched filter for a low correlation factor in the background ($K = 0.11$) are below those of the ACW augmented detector at $K = 0.89$. It should be noted that the TDLMS based ACW did not require any explicit model for the background clutter, and was able to adapt to the correlated components.

The same narrow band image was also passed through a local demeaning filter using a 4×4 window. The local demeaning filter has been found to produce Gaussian image statistics [8,9]. Further, the covariance of the output of local demeaning filters has been found to be very close to the identity matrix [8,9]. This makes the local demeaning algorithm a likely candidate for whitening filters. However, for narrow band images with a strong frequency component away from the zero frequency (in the 2-D spatial frequency domain) the local demeaning filter is not able to remove the high frequency components of the clutter. Figure 8 shows the output of the local demeaning filter. The spectrum (shown in Fig.9) of this output shows the presence of the sinusoidal clutter as the narrow band interference. If the window size of the local demeaning filter is chosen larger than 4×4, the local mean approaches the global mean and the performance of the local demeaning filter degrades.

3.3 Bounds on μ

The distinction between the clutter and the signal of interest is accomplished on the basis of the differences in the correlation lengths of the signal and the background clutter. The rate of adaptation of the TDLMS filter depends very strongly on the value of the adaptation parameter μ. Hence, the issue of predicting only the background clutter and ignoring the

presence of the signal in its prediction is critically dependent on the choice of μ.

If λ_{min} and λ_{max} are the largest and smallest eigenvalues of the autocorrelation matrix $\mathbf{R}$ defined in Eq.4, then the number of iterations, d_a, required by the filter to adapt is bounded by [29]

$$\frac{-1}{ln\,(1 - \mu\lambda_{max})} \leq d_a \leq \frac{-1}{ln\,(1 - \mu\lambda_{min})} \tag{28}$$

Since the the filter weights should converge to the statistics of the noise but not to those of the signal of interest, μ should be chosen such that the *spatial extent* of the signal, d_s satisfies

$$d_s \ll \frac{-1}{ln\,(1 - \mu\lambda_{s,max})} \tag{29}$$

where, $\lambda_{s,max}$ is the largest eigenvalue of the signal "autocorrelation" matrix. Thus if μ is chosen such that

$$\mu \ll \frac{1 - e^{-1/d_s}}{\lambda_{s,max}} \tag{30}$$

and lies within the bounds in Eq.28, the filter will be able to predict the background clutter but not the signal of interest, and thus separate the two. It is obvious that a lower value of μ will lead to more of the energy from the signal to be output in the error channel, at the same time μ should high enough to converge to the background clutter statistics. Further as μ is increased, the misadjustment noise increases and the filter performance will degrade. Thus it is expected that for any given set of clutter and signal correlation characteristics, there will be an optimum value of μ which will give a maximum gain in the TDLMS output. This will be experimentally seen in section 5.

4   Reduction in Number of False Alarms

The performance of a TDLMS prewhitening adaptive filter for nonideal backgrounds is studied in this section. To characterize the improvement obtained by the use of a TDLMS prewhitener, the false alarm rate of such a detector is used as a metric.

Images consisting of single pixel signals of various intensities embedded in a cloud were generated. The cloud background was generated[2] using the random midpoint displacement

---

[2]The program used for generating the clouds was developed by Om Sharma now at the Goddard Space Flight Center, Greenbelt, MD.

generation technique for fractals which is often used for scene generation and cloud modeling [30,31]. The correlation characteristics of such backgrounds was examined and found to be similar to the 2-D Gaussian model developed by Chan et. al. [4]. Fig.10 shows the input with 20 objects inserted at random points with random input signal to noise ratios. Fig.11 shows the output from the TDLMS (filter window of 3×3 and $\mu = 1e - 7$) after most of the background cloud has been cancelled and the residual output contains the signals of interest.

The detectability of the signal of interest depends on the signal to background ratio in its local region and we define the *local signal to background ratio* (LSBR) as the signal to background ratio in a window around the region of interest. Thus, if the window of interest is a rectangular region defined by (L_x, L_y) to (H_x, H_y), then the LSBR (in dB) is defined as

$$LSBR = 10 \log_{10} \frac{\sum_{i=L_x}^{H_x} \sum_{j=L_y}^{H_y} (\mathbf{I}(i,j) - m_w)^2}{\sigma_w^2} \tag{31}$$

where, m_w is the mean of the background in the window of interest and σ_w is the variance in the same window.

Since the background statistics vary across the image, the LSBR gain is not directly related to the input signal amplitude. Table 1 details the signal to background ratio gains for the 20 pixels of interest. A threshold for *perfect detection* can be defined as the highest threshold at which the weakest signal of interest is detected. For this image it was found that the number of false alarms per pixel of the image, at the threshold of perfect detection, is reduced from 0.74 to 0.12 after processing with the TDLMS adaptive filter. It is thus seen that the background clutter is predicted very well by the TDLMS filter with a vast improvement in the *detectability* of the signals.

To characterize this further, the number of false alarms for a single object in this clutter was found for varying input signal intensities, at a single location in the image with the use of a 3×3 TDLMS adaptive filter. A one pixel object was inserted at the pixel location (100,100) and detection was done by thresholding the output image to the intensity value of the object pixel at the residual output. This is the highest threshold that could be used for the detection of the inserted object. At this threshold the number of false alarms in the image were found. Fig.12 shows the change in the number of false alarms per pixel

of the output image as a function of the input LSBR for two different values of μ. The unprocessed image, due to the dim nature of the object and low LSBR, has a very high number of false alarms. The TDLMS whitening filter shows a vast improvement (both for the $\mu = 10^{-7}$ and the $\mu = 10^{-6}$ cases) with the number of false alarms in the image going to zero as the LSBR increases. As expected, the number of false alarms is less for $\mu = 10^{-7}$ than for the $\mu = 10^{-6}$ case, since the lower μ permits better separation of the components of a signal based on their correlation lengths. The equivalent false alarm number for two different local demeaning filters is also shown. The local demeaning filters with window sizes of 9x9 or 7x7 show a reduction in the number of false alarms as the LSBR increases. However for very low LSBR the local demeaning filter has significantly high number of false alarms.

5 Performance with TIMS Sensor Data

In this section we present the results obtained by applying this two stage augmented detector to infrared image data. The image used is channel 4 of a 6 channel data set collected by the NASA Thermal Infrared Multispectral Scanner(TIMS) sensor and includes a rural background over the hills of Adelaide, Australia [12]. This section includes performance data from both real and injected point objects in TIMS sensor output data. The injected objects were utilized to illustrated the performance of the TDLMS filter for known object parameters.

5.1 Dependence on the Adaptive Time Constant

Fig.13 shows the behavior of 3×3 TDLMS filter as a function of μ for a one pixel signal at two different signal intensities. As described in section 3.4, there is an optimum value of μ at which the maximum gain is obtained. If μ is less than this optimum value, the filter is not able to converge to the statistics of the clutter. Hence the residual channel contains some component of the correlated clutter leading to a reduced gain. If the value of μ is higher than the optimum, the adaptive filter is very sensitive to changes in the input, and some of the energy from the signal of interest is also predicted and cancelled. The misadjustment noise in the adaptive filter weights increases with μ and is another factor contributing to

the drop in gain as μ increases.

5.2 Separation by Differences in Correlation Lengths

To study the ability of the TDLMS prewhitener to separate signals based on spatial correlation, simulation studies were conducted with varying signal spread. Two objects with symmetric Gaussian intensity functions defined by Eq.21 were inserted in the infrared background. The value of $\sigma^2(= \sigma_x^2 = \sigma_y^2$) defines the spread of the object intensity. A higher σ^2 leads to a more spatially spread signal. Fig.14 shows an image with the two components inserted in the background. One is the object of interest (at pixel location 100,100) which is a Gaussian shape with $\sigma^2 = 2$ and the other is a component of the same shape but with $\sigma^2 = 98$. Fig.15 shows the output of the TDLMS whitener (filter size of 3×3 and $\mu = 1e - 7$) for this case, where the component of the input with $\sigma^2 = 2$ is seen to be present, while the output for the $\sigma^2 = 98$ case is absent.

Figure 16 shows the energy at the pixel of interest in the residual channel output of the TDLMS filter as a function of the signal correlation length (σ^2). An object defined by Eq.21 was used and the pixel intensity at the output observed. It is seen that as the correlation length increases, the output energy at the pixel of interest decreases. Further, as shown in Fig.17, the energy in the prediction channel of the TDLMS filter correspondingly increases as the correlation length increases. It should be noted that the prediction channel output always contains the energy due to the non zero mean of the image which is seen in Fig.17 as a base level of 1.3×10^4.

In both these plots, three regions (depending on μ) can be defined for this TDLMS adaptive filter:

- (1) For objects with very small correlation length, the energy is contained almost totally in the output channel.

- (2) For objects of long correlation length, the energy is absent from the output.

- (3) For objects of intermediate correlation length, there is a partial decorrelation between the input and reference channels. In such cases the energy of the object is split between both channels.

15

A similar plot for the local demeaning filter is shown in Fig.18, and it is seen that the local demeaning filter is not able to provide a clear boundary between the two regions of differing correlation spread. Thus we see that the TDLMS is able to separate the object of interest from the clutter based on their correlation spread.

5.3   Detection of Small Objects in Spatially Correlated Clutter

In [12] Hoff et. al. identified 14 pixels which contained small objects in the TIMS sensor data described above. The 14 pixels were identified on the basis of multispectral data in the 6 separate bands. The locations designated in [12] are illustrated in by boxes in Fig.19. The pixel intensities at the output of the TDLMS filter (residual channel) is shown in Fig.20. A 3×3 TDLMS filter with $\mu = 10^{-7}$ was used. Table 6 describes the input and output signal to background ratios for these pixels. Note that the gain is very nonuniform across the image. This is a result of variations in the LSBR across the image.

Fig.21 shows a high resolution intensity plot around the 13th object defined in Table 6. As seen in the figure and described in the table, this object has a very high LSBR. This causes the object to be predicted. Fig.22 shows the corresponding output for this pixel. It is seen that there are a number of pixels in the local region with comparable intensity.

Fig.23 is a similar high resolution plot around the 14th object defined in Table 6. In this case, due to the low LSBR, the output (shown in Fig.24) is seen to contain energy due to the object pixel and there is a vast improvement in the detectability. This is also seen in the LSBR gain for this pixel as seen in Table 6.

Though there is a loss in LSBR at some pixels it is seen that the detection performance of the filter improves considerably when the input image is processed by the TDLMS adaptive filter. For a threshold set to detect all 14 of the signal mentioned in Table 6, the number of false alarms in the image is significantly reduced. If the detection criterion is changed to reduce the number of detected objects the number of false alarms in the image are further reduced. A plot of the percentage of objects detected as a function of the number of false alarms per pixel is shown in Fig.25. A similar plot for the local demeaning filter is also shown in this figure and it is seen that for a fixed number of false alarms per pixel the percentage of of objects detected is much higher when the data is processed with the TDLMS based adaptive filter than with the local demeaning filter.

6   Conclusions

The TDLMS adaptive prediction filter was applied to the problem of detecting objects in image data. It is seen that for correlated inputs, the TDLMS filter weights converge to the solution of the two dimensional Wiener-Hopf equation. This leads to the clutter in the image being predicted thereby allowing the signal of interest to be enhanced relative to the background clutter. For an ideal two dimensional sinusoidal input as clutter, the filters weights were shown to be sinusoidal, analogous to the one dimensional filter. It was shown that the TDLMS based filter creates a notch in the spatial frequencies of the narrow band clutter.

On simulated cloud data and in TIMS sensor data containing small objects at known locations, it was also shown that the number of false alarms is significantly reduced when the input is preprocessed with the TDLMS filter. The separation of the signal of interest from the clutter was seen to depend on the energy of the signal and the difference in correlation length between the background and the object of interest. It is seen that the gain obtained by prewhitening depends on the local correlation characteristics of the image around the pixel of interest.
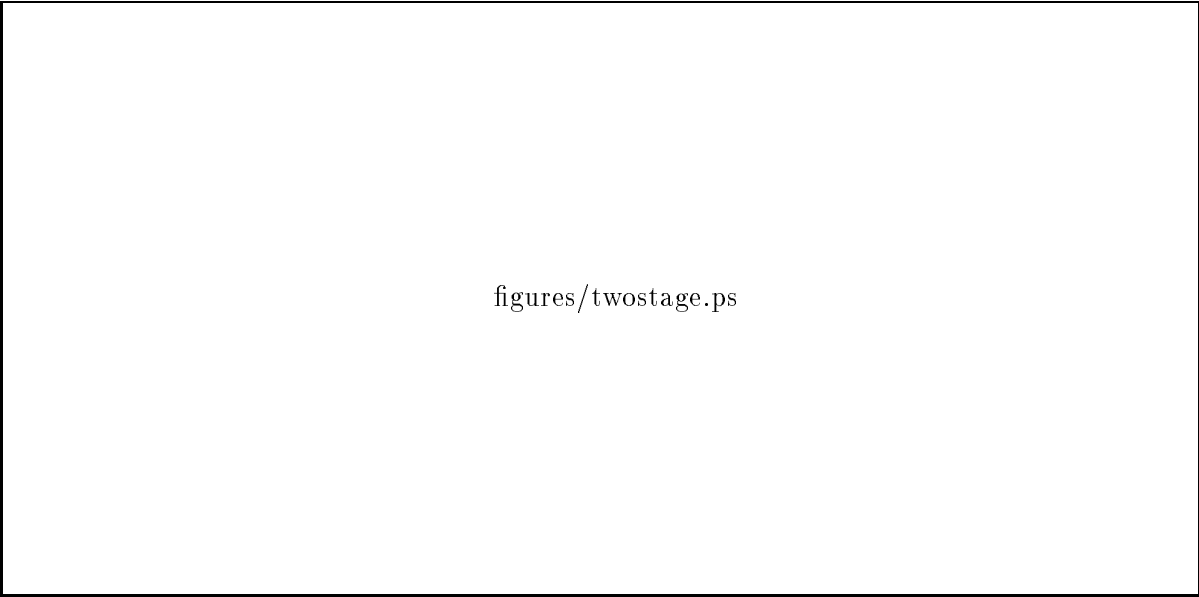
References

[1] C. W. Therrien, T. F. Quatieri, and D. E. Dudgeon, "Statistical Model-Based Algorithms for Image Analysis," *Proceedings of the IEEE*, vol. 74, pp. 532–551, Apr. 1986.

[2] A. K. Jain, *Fundamentals of Digital Image Processing*. Englewood Cliffs, NJ.: Prentice Hall, 1989.

[3] A. K. Jain, "Advances in Mathematical Models for Image Processing," *Proceedings of the IEEE*, vol. 69, pp. 502–528, 1981.

[4] D. S. K. Chan, D. A. Langan, and D. A. Staver, "Spatial Processing Techniques for the Detection of Small Targets in IR Clutter," in *Proc. of SPIE, Technical Symposium on Optical Engineering and Photonics in Aerospace Sensing*, (Orlando, Florida), Apr.,1990.

[5] R. Nitzberg, E. H. Takken, D. Friedman, and A. F. Milton, "Spatial Filtering Techniques for IR Sensors," in *Proc. of SPIE, Technical Symposium on Smart Sensors*, vol. 178, 1979.

[6] E. H. Takken, D. Friedman, A. F. Milton, and R. Nitzberg, "Least-mean-square Spatial Filter for IR Sensors," *Applied Optics*, vol. 18, no. 24, pp. 4210–4222, 1979.

[7] M. S. Longmire and E. H. Takken, "LMS and Matched Digital Filters for Optical Clutter Suppression," *Applied Optics*, vol. 27, no. 6, pp. 1141–1159, 1988.

[8] J. Y. Chen and I. S. Reed, "A Detection Algorithm for Optical Targets in Clutter," *IEEE Transactions on Aerospace and Electronic Systems*, vol. 23, no. 1, pp. 46–59, 1987.

[9] A. Margalit, L. S. Reed, and R. M. Gagliardi, "Adaptive Optical Target Detection Using Correlated Images," *IEEE Transactions on Aerospace and Electronic Systems*, vol. 21, pp. 394–405, May 1985.

[10] D. Wang, "Adpative Spatial/Temporal/Spectral Filters for Background Clutter Suppression and Target Detection," *Optical Engineering*, vol. 21, pp. 1033–1038, Dec. 1982.

[11] A. Adridges, G. Cook, S. Mansur, and K. Zonca, "Correlated Background Adaptive Clutter Suppression and Normalisation Techniques," in *Proc. of SPIE, Multispectral Image processing and Enhancement*, vol. 933, 1988.

[12] L. E. Hoff, J. R. Evans, and L. E. Bunney, "Detection of Targets in Terrain Clutter by Using Multispectral Infrared Image Processing," *Technical Report for Naval Ocean Systems Center*, Dec. 1990.

[13] H. Wang and L. Cai, "On Adaptive Multiband Signal Detection with the SMI Algorithm," *IEEE Transactions on Aerospace and Electronic Systems*, vol. 26, pp. 768–773, May 1990.

[14] J. R. Zeidler, "Performance analysis of LMS Adaptive Prediction filters," *Proceedings of the IEEE*, vol. 78, pp. 1781–1806, Dec. 1990.
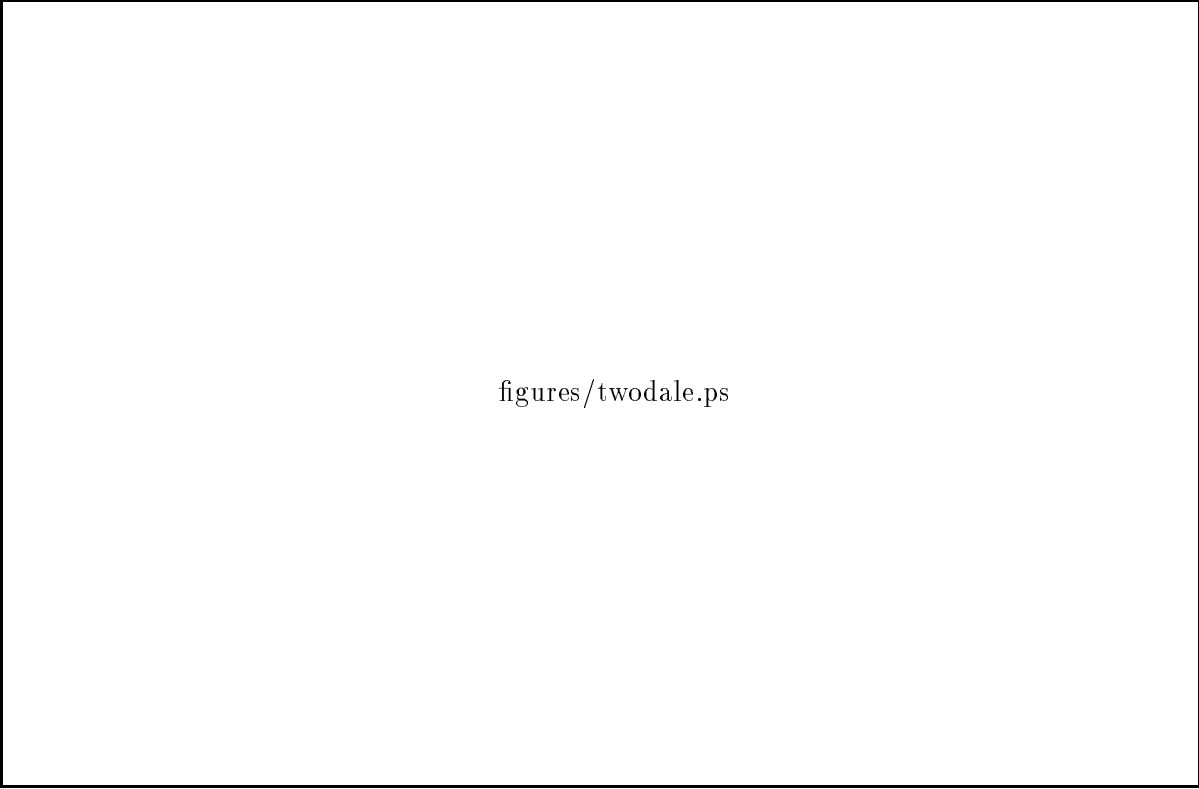
[15] J. T. Rickard, J. R. Zeidler, M. J. Dentino, and M. Shensa, "A Performance Analysis of Adaptive Line Enhancer-Augmented Spectral Detectors," *IEEE Transactions on Acoustics, Speech, and Signal Processing*, vol. ASSP-29, pp. 694–701, June 1981.

[16] L. Milstein, "Interference Rejection Techniques in Spread Spectrum Communications," *Proceedings of the IEEE*, vol. 76, pp. 657–671, June 1988.

[17] G. A. Clark and P. W. Rodgers, "Adaptive Prediction Applied to Seismic Event Detection," *Proceedings of the IEEE*, vol. 69, pp. 1166–1168, Sep. 1981.

[18] N. Ahmed, R. J. Fogler, D. L. Soldan, G. R. Elliott, and N. A. Bourgeois, "On An Intrusion Detection Approach Via Adaptive Prediction," *IEEE Transactions on Aerospace and Electronic Systems*, vol. 15, pp. 430–437, May 1979.

[19] M. M. Hadhoud and D. W. Thomas, "The Two-Dimensional Adaptive LMS(TDLMS) Algorithm," *IEEE Transactions on Circuits and Systems*, vol. 35, no. 5, pp. 485–494, 1988.

[20] M. Ohki and S. Hashiguchi, "Two-Dimensional LMS Adaptive Filters," *IEEE Transactions on Consumer Electronics*, vol. 37, pp. 66–73, Feb. 1991.

[21] M. Ohki and S. Hashiguchi, "A New 2-D LMS Adaptive Algorithm," in *Proceedings IEEE International Conf. on Acoustics Speech and Signal Processing*, vol. 4, (Toronto, Canada), pp. 2113–2116, April 1991.

[22] H. Youlal, M. Janati-i, and M. Najim, "Two-Dimensional Joint Process Lattice For Adaptive Restoration of Images," *To be Published in the IEEE Transactions on Image Processing*, July 1992.

[23] W. B. Mikhael and S. M. Ghosh, "Two-Dimensional Block Adaptive Filtering Algorithms," in *Proceedings IEEE International Symposium on Circuits and Systems*, no. 3, pp. 1219–1222, May 1992.

[24] A. Whalen, *Detection of Signals in Noise*. New York: Academic Press, 1971.

[25] J. R. Zeidler, E. H. Satorius, D. M. Chabries, and H. T. Wexler, "Adaptive Enhancement of Multiple Sinusoids in Uncorrelated Noise," *IEEE Transactions on Acoustics, Speech, and Signal Processing*, vol. ASSP-26, pp. 240–254, June 1978.

[26] A. Nehorai and M. Morf, "Enhancement of Sinusoids in Colored Noise and the Whitening Performance of Exact Least Squares Predictors," *IEEE Transactions on Acoustics, Speech, and Signal Processing*, vol. ASSP-30, pp. 353–363, June 1982.

[27] C. M. Anderson, E. H. Satorius, and J. R. Zeidler, "Adaptive Enhancement of Finite Bandwidth Signals in White Gaussian Noise," *IEEE Transactions on Acoustics, Speech, and Signal Processing*, vol. 31, pp. 17–28, Feb. 1983.

[28] J. T. Rickard and J. R. Zeidler, "Second Order Output Statistics of the Adaptive Line Enhancer," *IEEE Transactions on Acoustics, Speech, and Signal Processing*, vol. ASSP-27, pp. 31–39, Feb. 1979.

[29] S. Haykin, *Adaptive Filter Theory.* Englewood Cliffs, NJ: Prentice-Hall, 1985.

[30] B. B. Mandelbrot, *The Fractal Geometry of Nature.* New York: W. H. Freeman and Co., 1982.

[31] H. O. Peitgen and D. Soupe, *The Science of Fractal Images.* New York: Springer-Verlag, 1988.

figures/twostage.ps

Figure 1: **A Two Stage Filtering and Detection Procedure.**

figures/twodale.ps

Figure 2: **A Two Dimensional Adaptive Filter.**
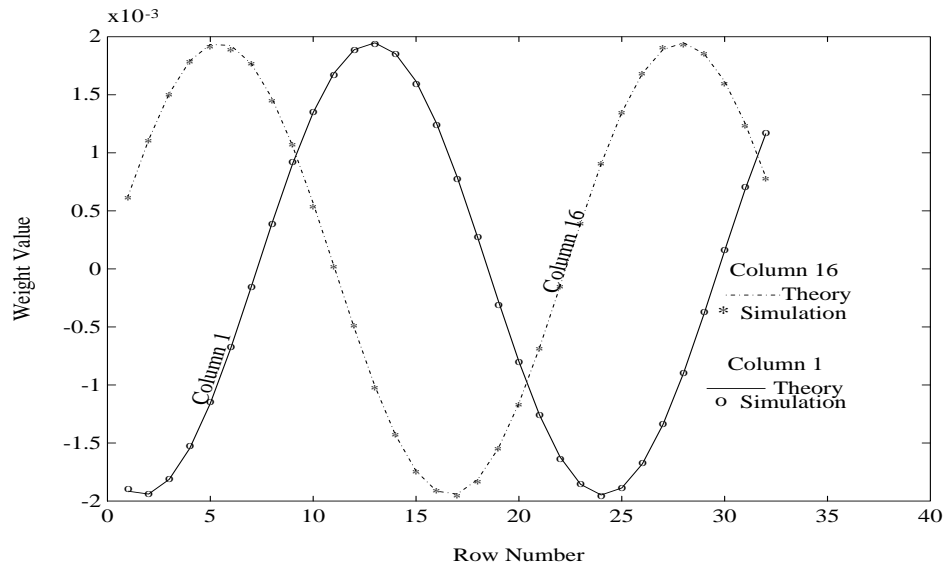
Figure 3: **Two columns of the weight matrix : The simulation was done with a 32x32 TDLMS filter with $\mu = 1e-8$ and the weights after convergence are seen to agree with the theoretical expression.**
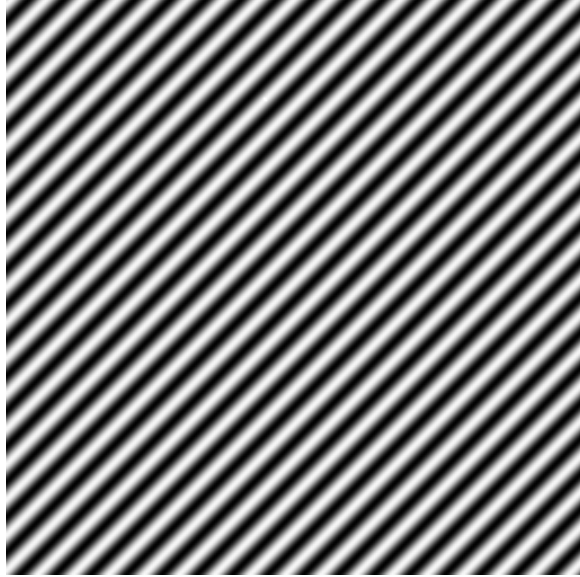
(a) Input at LSBR=9.41dB
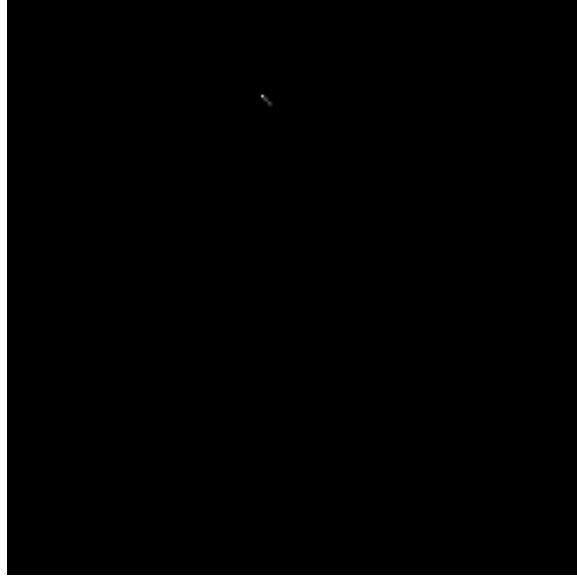
(b) **Output from the residual channel of the TDLMS Filter: LSBR = 27.18dB**

Figure 4: **Sinusoidal Clutter with small object signal at (115,45) with** $K = 1$
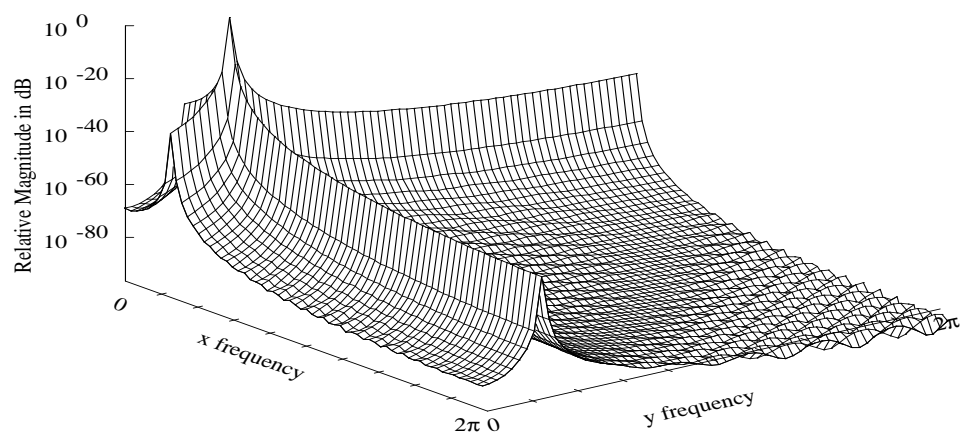
Figure 5: **Spatial 2-D FFT of the signal in Sinusoidal Clutter (Log Magnitude Plot).**
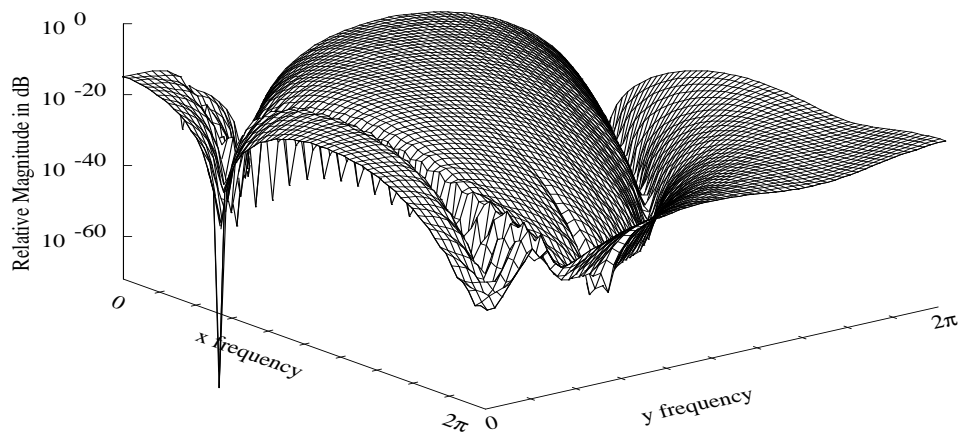
Figure 6: **Spatial 2-D FFT of the Output (Residual) of the TDLMS filter (Log Magnitude Plot).**
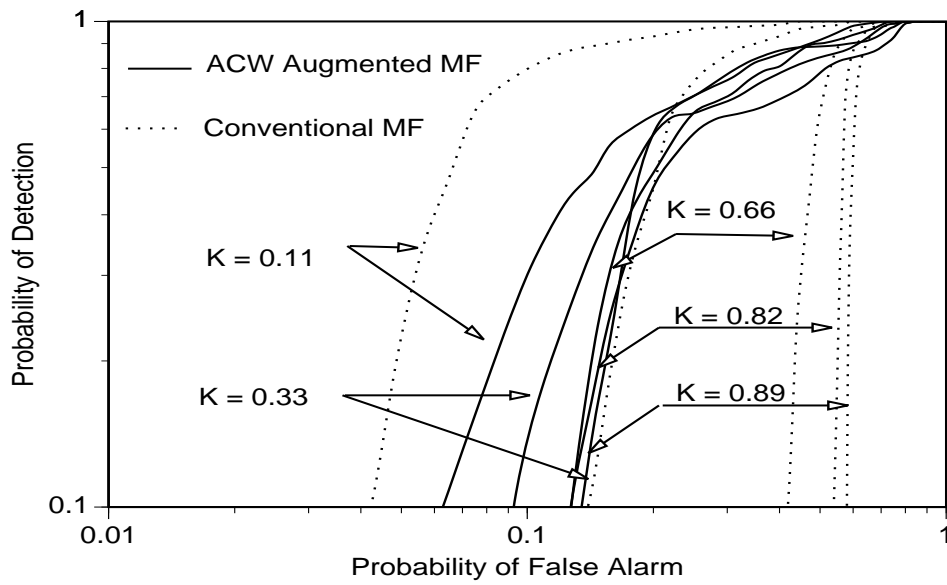
Figure 7: **The Operating Characteristics of a detector augmented by an Adaptive Clutter Whitener at PSBR = -27.55 dB.**
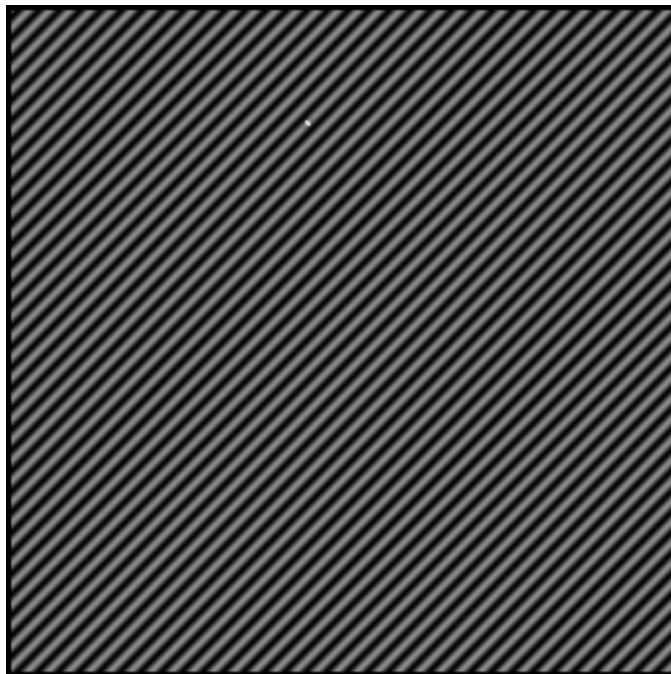
Figure 8: **The Output of a 4x4 local demeaning filter LSBR = 10.78dB (Signal of interest is at (115,45)) .**
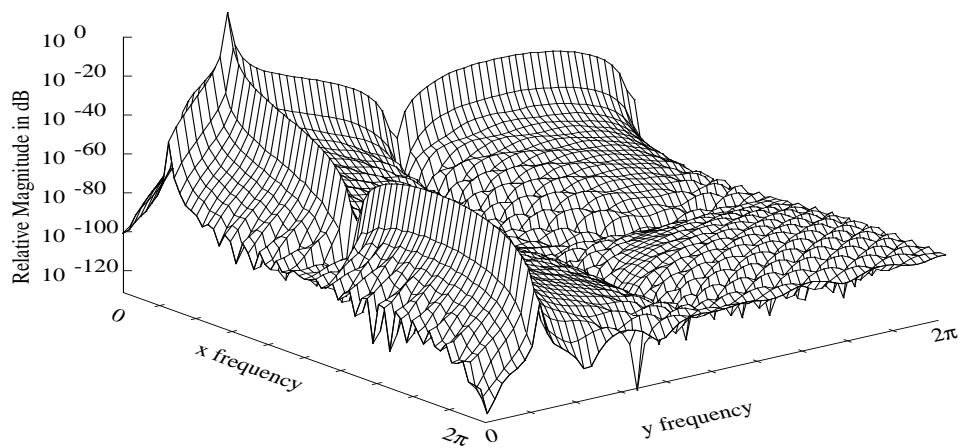
Figure 9: **Spatial 2-D FFT of the Local Demeaning Filter Output (Log Magnitude Plot).**
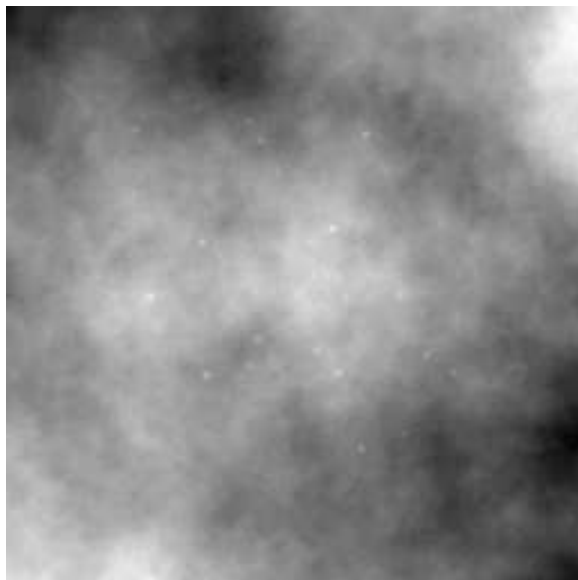
Figure 10: **Cloud with 20 signals inserted at random: Input to TDLMS Filter.**
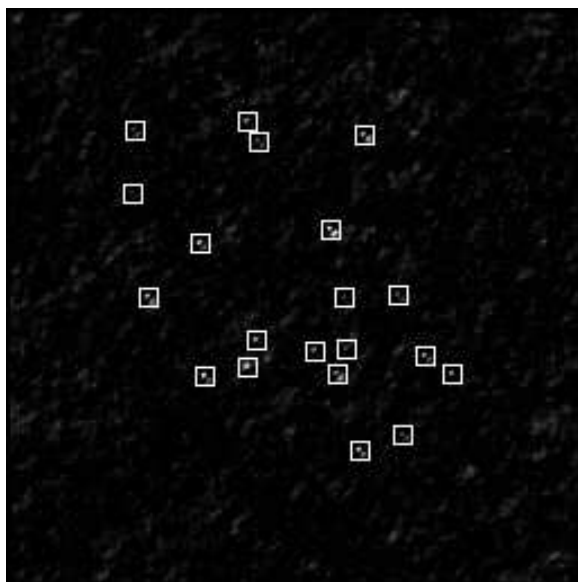
Figure 11: **Cloud with 20 signals: Output Energy in TDLMS Filter Residual.**

Location		LSBR in (dB)		LSBR Gain
x	y	Input	Output	in dB
83	57	5.126	14.185	9.059
152	152	2.611	13.803	11.192
160	108	5.257	17.453	12.196
128	175	6.972	16.336	9.364
55	58	6.064	14.225	8.161
129	151	-3.853	-2.696	1.157
51	108	4.046	18.604	14.558
60	113	8.405	14.866	6.461
153	138	7.852	19.242	11.390
190	177	5.559	12.718	7.159
129	64	12.235	16.990	4.755
148	112	5.051	18.667	13.616
155	187	6.469	18.502	12.033
164	89	12.225	18.894	6.669
57	160	9.217	16.128	6.911
99	145	12.999	17.179	4.18
163	199	9.671	17.199	7.528
105	87	10.116	16.872	6.756
197	158	13.152	19.159	6.007
163	148	10.744	14.434	3.69

Table 1: **20 Randomly inserted signals into the cloud image, with the input and output statistics ($\mu = 10^{-7}$).**
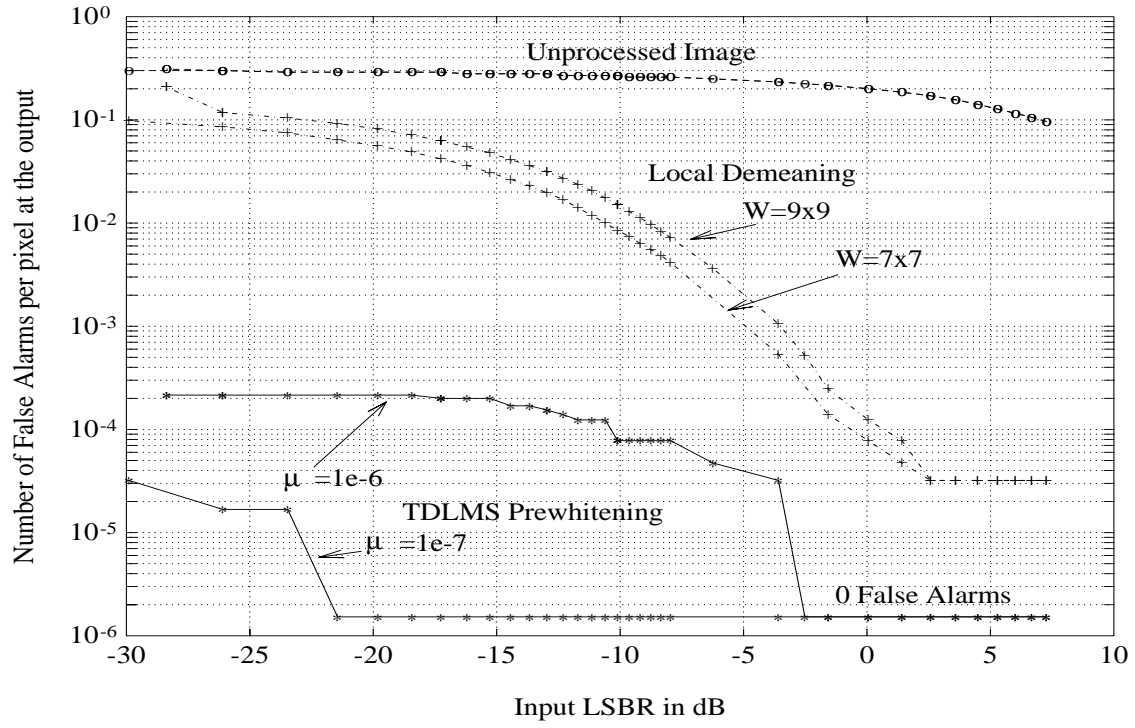
Figure 12: **Cloud with single object at (100,100). False detections per pixel in the image, for perfect detection as the signal LSBR changes.**
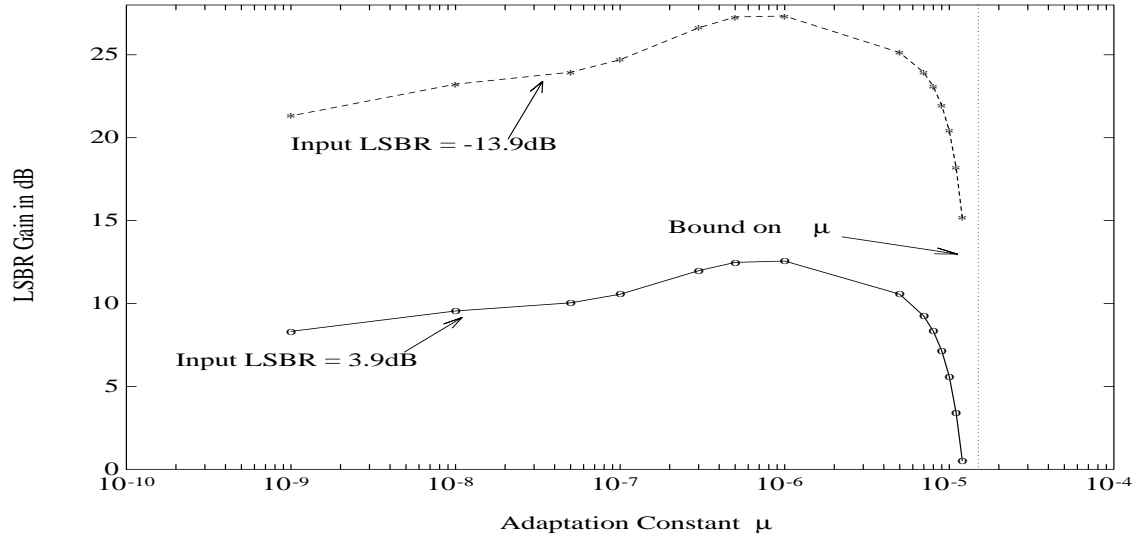
Figure 13: **Gain vs. μ for the Adelaide background with one pixel signal at (100,100).**
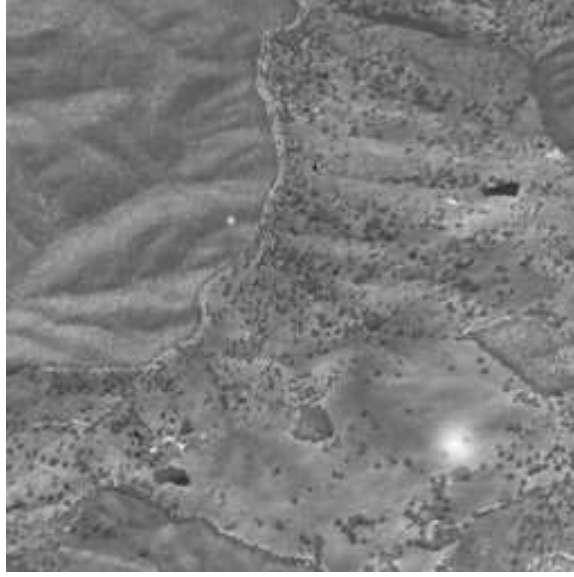
Figure 14: **Signal with two components: object of interest at (100,100) with correlation spread of $\sigma^2 = 2$ and spurious component at (200,200) with correlation spread of $\sigma^2 = 98$.**
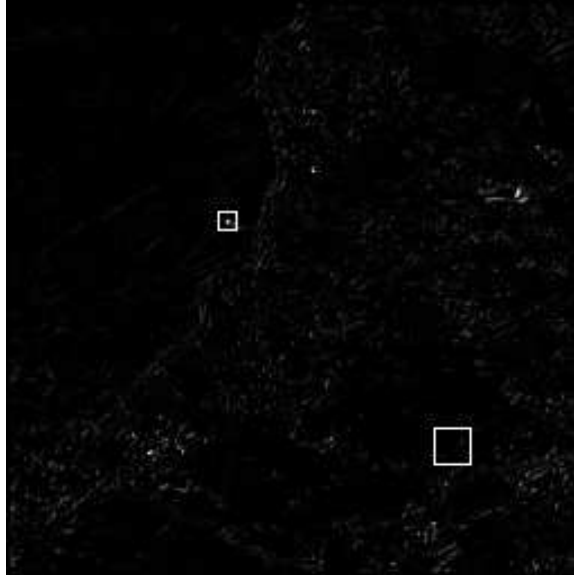
Figure 15: **The residual channel output for Fig.15. TDLMS was used with a 3x3 window and $\mu = 1e - 7$. LSBR at (100,100) = 16.024dB and LSBR at (200,200) = -16.75dB.**
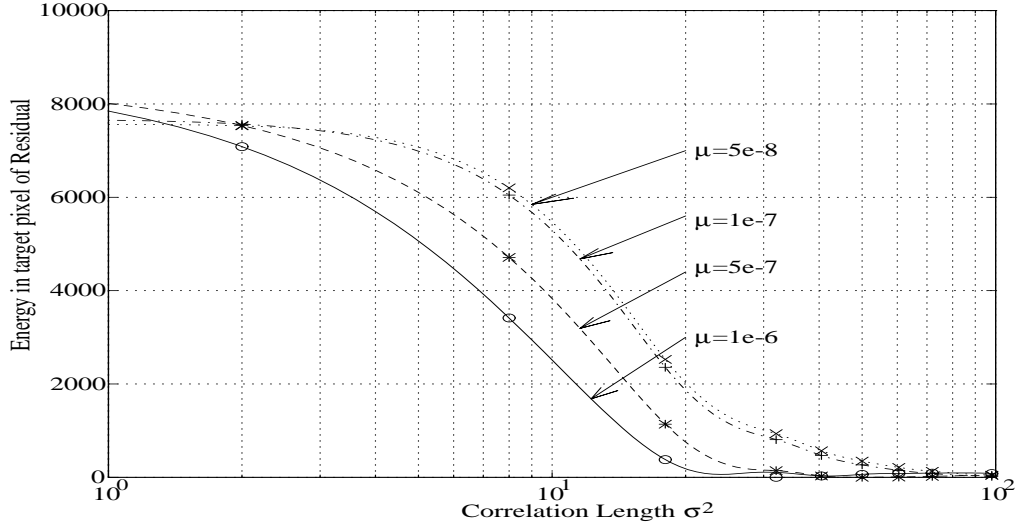
Figure 16: **Energy at the pixel of interest in the output of the TDLMS as a function of the correlation length.**
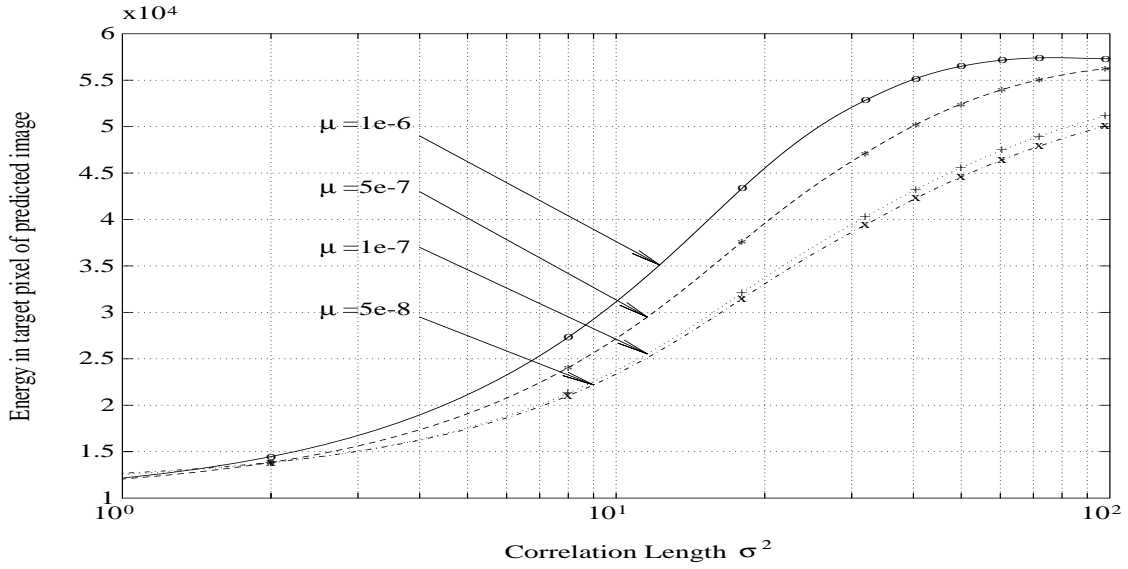
Figure 17: **Energy at the pixel of interest in the prediction channel of the TDLMS as a function of the correlation length.**
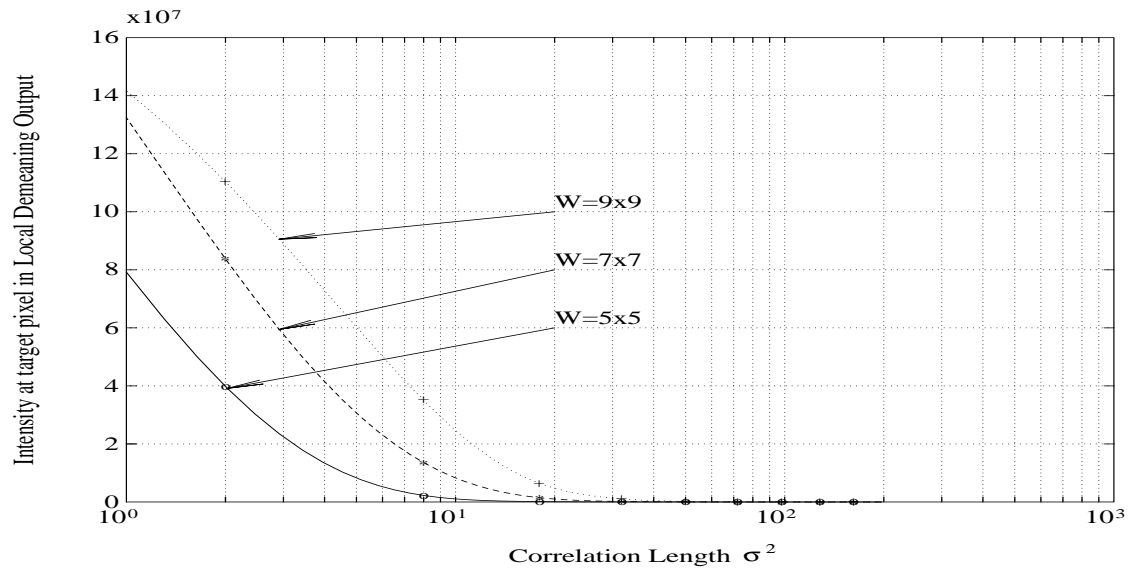
Figure 18: **Energy at the pixel of interest in the output of the Local De-meaning filter as a function of the correlation length.**
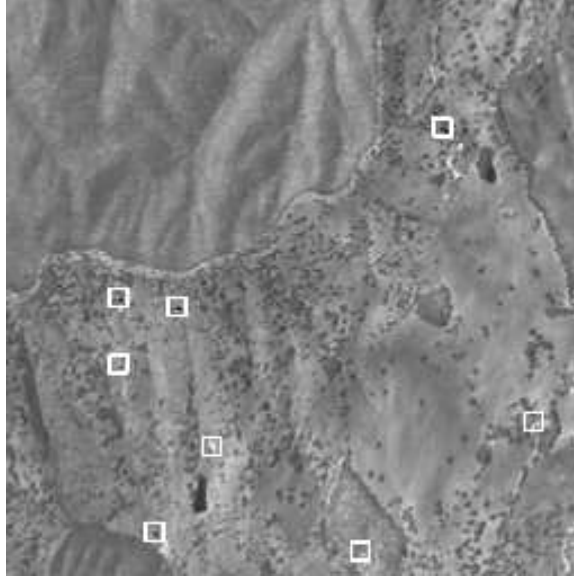
Figure 19: **The infrared image data with the 14 pixels of interest. Note that some objects are clustered close to each other their enclosing boxes overlap.**
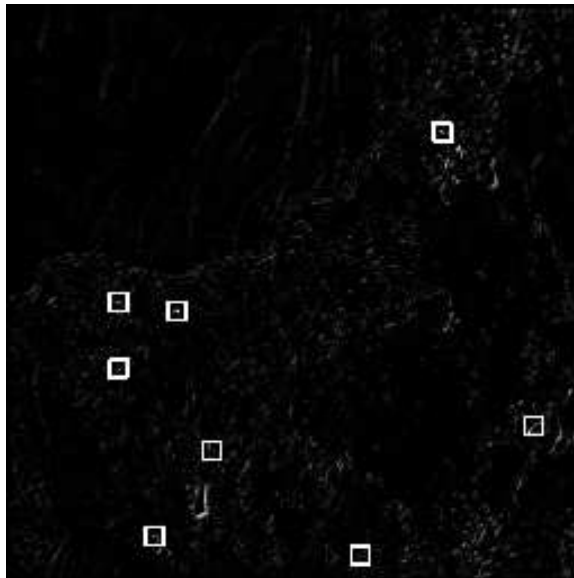
Figure 20: **The infrared image data output from TDLMS adaptive fiter for Fig.20.**

| Location | | Signal | Background | LSBR in (dB) | | LSBR Gain |
x	y	Energy	Energy	Input	Output	in dB
133	50	594	501.97	0.7291	12.6507	11.9216
133	51	0.4414	493.27	-30.4829	11.8246	42.3074
137	76	13.453	334.868	-13.9606	13.5457	27.5063
137	77	2187	342.05	8.0567	16.6005	8.5438
162	51	2103	367.06	7.5810	7.7111	0.1302
163	50	934	405.636	3.6219	9.6000	5.9781
57	194	52.3	553.56	-10.2467	13.0149	23.2616
58	195	10386	710.61	11.6483	10.7177	-0.9306
237	66	11.31	714.05	-18.0020	13.4291	31.4310
237	67	836	721.38	0.6414	8.2041	7.5627
245	158	124	293.53	-3.7509	1.4168	5.1678
246	158	88.06	315.05	-5.5360	8.0799	13.6158
199	92	10406	664.67	11.9468	-6.6192	-18.5659
188	235	65.5	864.01	-11.2025	7.3820	18.5845

Table 2: **The input and output statistics of pixels declared as objects of interest in the Adelaide image data ($\mu = 10^{-7}$).**
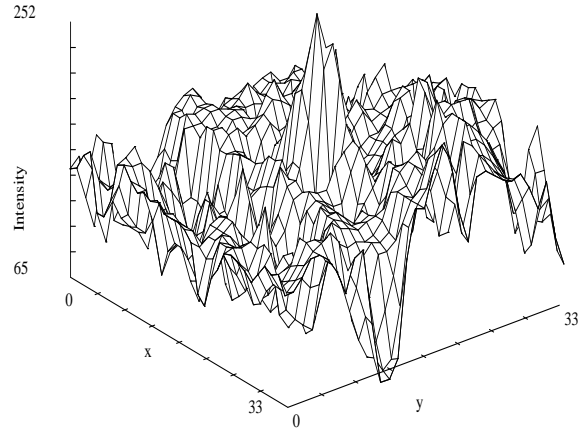
Figure 21: **High resolution intensity plot of a 33x33 window around the pixel (199,92) before processing.**
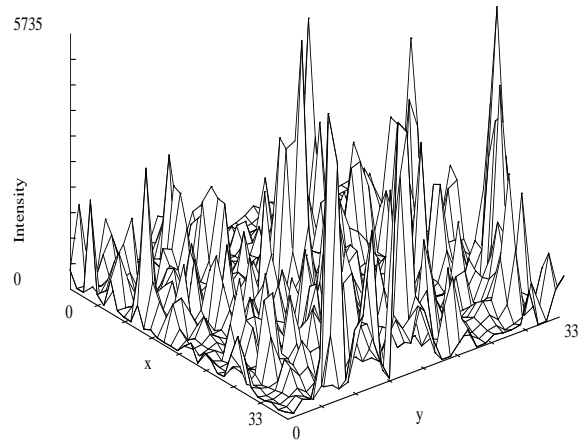
Figure 22: **High resolution intensity plot of a 33x33 window around the pixel (199,92) after processing.**
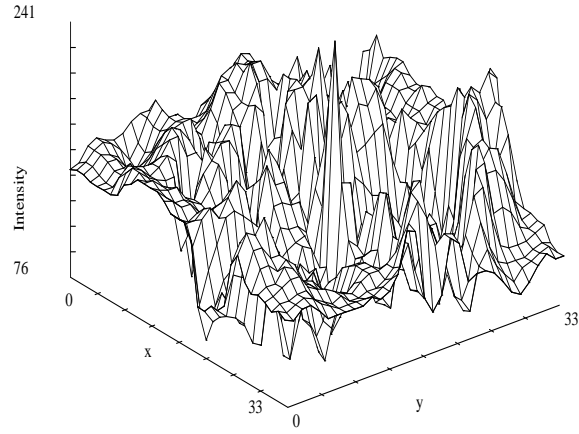
Figure 23: **High resolution intensity plot of a 33x33 window around the pixel (188,235) before processing.**
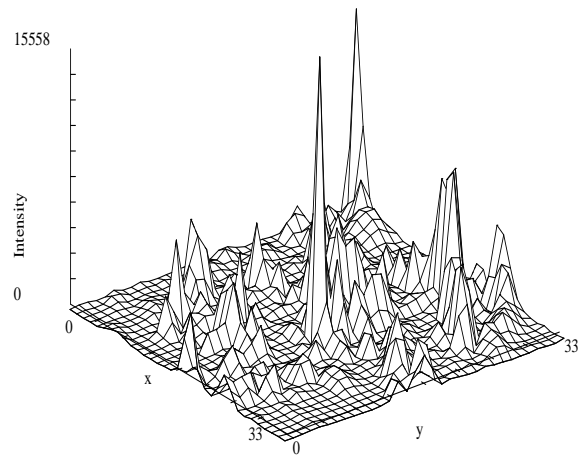
Figure 24: **High resolution intensity plot of a 33x33 window around the pixel (188,235) after processing.**
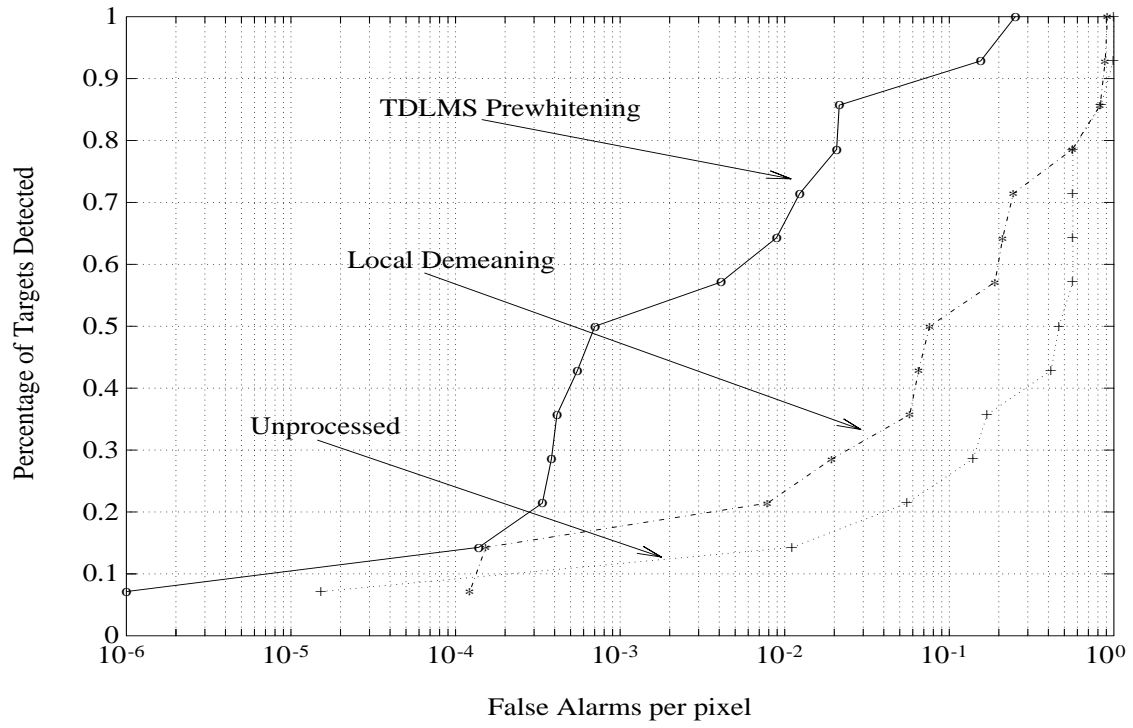
Figure 25: **False alarms in the Adelaide image for known objects as the percentage of objects detected is lowered. TDLMS was used with** $\mu = 1e - 7$.

List of Figures